國 立 中 央 大 學

物 理 學 系
碩 士 論 文

VUV and EUV irradiation of CH_4+NH_3 ice mixtures

研究生: Leung Pui Shan

指導教授: Chen Yu Jung

中 華 民 國 一 百 零 六 年 十 二 月

國 立 中 央 大 學

物 理 學 系
碩 士 論 文

VUV and EUV irradiation of CH$_4$+NH$_3$ ice mixtures

研究生: Leung Pui Shan

指導教授: Chen Yu Jung

中 華 民 國 一 百 零 六 年 十 二 月

VUV and EUV irradiation of CH$_4$+NH$_3$ ice mixtures

中文摘要

關鍵字：星際冰晶，冥衛一，眞空紫外光，超眞空紫外光

我們永遠不會停止對外太空的探索。自二十世紀以來，天文學家們一直在天空中觀察生命的起源。除了觀測恆星以外，我們現在可以模擬外太空環境，在地球上的實驗室中製造一些簡單的分子。爲了研究CN$^-$的形成，我們將CH$_4$和NH$_3$（由Kim和Kaiser（2011）[?]提出的機制）進行沉積以模擬冥衛一(Charon)表面。我們提供VUV和EUV輻射作爲能源，主要使用傅里葉變換紅外光譜（FTIR）和四極桿質譜（QMS）來研究不同濃度的CH$_4$和NH$_3$冰混合物。

VUV and EUV irradiation of CH_4+NH_3 ice mixtures

英文摘要

Keywords: interstellar ice, Charon, VUV irradiation, EUV irradiation

We never stop the exploration of the outer space. Since 1900s, astronomers have observed all over the sky to seek origin of life. Apart from observing stars, we may simulate the outer space environments and make some simple molecules in laboratories on the earth now. To investigate the formation of CN^-, we deposite CH_4 and NH_3 (mechanism proposed by Kim and Kaiser (2011)[**?**]) at 15 K and 1×10^{-10} torr to simulate the surface of Charon. We provide VUV and EUV irradiations as energy sources and mainly use Fourier Transform Infrared Spectrometer (FTIR) and Quadrupole Mass Spectroscopy (QMS) to study different concentrations of CH_4 to NH_3 ice mixtures.

VUV and EUV irradiation of CH$_4$+NH$_3$ ice mixtures

謝誌

在我的求學生涯中，有很多的老師。不過，讓我得益最多的還是這兩年多的碩士生涯。

還記得剛剛來台灣的時候，半個人都不認識，憑著老師一封電郵就來台灣唸書，實在是人生路不熟。 這兩年裡面，最感謝的人就是我的指導教授，陳俞融老師。 雖然老師對我並沒有好臉色，每次我報告完總是一副"奇怪，你怎麼又離題了"的樣子；但是我知道責之深愛之切，每次打開老師的面書，就會知道：喔，這次老師又要生我的氣了。

在整個碩士生涯中，我學會最多的就是如何篩選一篇相關的文獻，怎樣和我自己的論文相比較，從而得出究竟這篇文獻是否適用的過程。從一開始不會把整篇文獻看完，到後來認真地仔細地看別人引用的文章，再到後來自己寫出來的時候該如何引用。或者我的論文內容並不充實，但我認為碩士課程需要學習的就是如何有辨別文獻的相關性。並不是以偏概全，嘩眾取寵，而是只把自己有把握的地方撰寫出來。

本論文得以完成，實在是一件非常不容易的事情。由於本人英文寫作不佳，所以感謝好友Jess幫忙修改英文句子。謝謝學長samuel教我使用Latex，謝謝實驗室的學長豆花教導我做實驗，學弟妹謝妮恩，蘇映全，在同步輻射期間的幫忙。Thanks Angela, Guillermo and Michel for your valuable comments on my thesis, which actually helps. Finally, thanks molview.org for providing an open source tool to creat 3D chemical models conviniently to make 3D diagrams.

Contents

List of Figures

List of Tables

1. Introduction

According to Hindu cosmological mythology, ancient people believe that a giant turtle bears the world on its back. Even after we stepped onto the moon at 1969, there are still plenty that we cannot explain. **CN^- plays an important role in life evolution because it is identified in comet 81P/Wild 2 brought back to earth analyzed by Kissel et al.(2004)[?]and comets are thought to preserve the "pristine" constituents in solar system.** The formation of CN^- is proposed by Kim and Kaiser (2001) [**?**],which is produced by ammonia (NH_3) and methane (CH_4). However, they have only demonstrated the effects of energetic electrons onto the ice mixtures, the photolysis experiments of CH_4+NH_3 ice mixtures especially variating relative proportions of CH_4 to NH_3 by VUV or EUV photons has not been performed. This thesis aims to investigate the chemistry of VUV and EUV irradiations on CH_4+NH_3 ice mixtures, which is possibly one of the main starting components to form CN^- in astrophysical environments.

NH_3 is often not probed in astrophysical environments unless detecting ambiguously because nearly all the infrared bands overlap with water **(suggested by d'Hendecourt and Allamandola (1986) [?])**. The "umbrella" mode (1070 cm^{-1}) is often obscured by the 10 micron silicate feature. It is often detected as ammonia hydrates ($NH_3 \cdot nH_2O$)[**?**]. The New Horizons team has revealed a high concentration crater of NH_3 on Charon[**?**]. Figure 1.1 presents the infrared spectra detected by LEISA camera regarding four different segments at the right panel. On Organa crater, we may observe a 2.2 μm absorption representing presence of ammonia at "b" spectrum. The part b spectrum is enlarged at left bottom panel with the green pigments indicates the concentration of ammonia overlapped on topological graph of Charon. This also explains

the different concentration of ammonia detected by different earth-based observation groups Cook et al (2007)[?] and Brown et al. (2000)[?].

Charon, as a member in the Pluto system, is the second massive member with masses about half of Pluto. It orbits around Pluto, where Pluto is orbiting the Sun with an semi-major axis of 39.1 A.U. and period of 248 earth years. Similar to the earth and moon system, they orbits synchronized to each other with tidal-lockings, which the same side always facing each other. The main ejecta from Pluto (5-6 $\times$ 10^{25} s^{-1} from the New Horizons observation) is CH$_4$ (99%), with net depositional flux of 4 $\times$ 10^{24} s^{-1} (98 % of which are CH$_4$) on Charon[?]. According to the New Horizons team, CH$_4$ from Pluto may accumulate onto the surface of Charon by cold-trapping which deposits at temperature below 25 K (at pressure 7.4 $\times$ 10^{-14} torr) onto the surface of Charon[?]. The amount of CH$_4$ varies along the surface of Charon because it depends on the length of time the temperature is below 25 K which in turns depends on diurnal motion and thermal inertia of Charon.

With obliquity of 119 degrees (currently) from the ecliptic, a long continuous darkness is expected. The upper panel of Figure 1.2 is the model simulated by Grundy et al. (2016)[?] presenting the surface temperature of Charon with respect to the lattitude and time in earth years. Based on length of time the surface temperature falls below 25 K, he plotted the length of time that CH$_4$ can accumulate onto Charon at the lower panel. From bottom panel, the mean cold-trap longitivity for depositing CH$_4$ is 2 times longer at the poles (130 earth years) than at 45° lattitude [?].The non-detection of methane by infrared spectra implies that its concentration is less than ammonia. However, the exact concentration ratios to ammonia was not fully modelled yet. Therefore, we decided to perform 3 relative ratios of CH$_4$ to NH$_3$ (in excess) to simulate the surface of Charon. They includes CH$_4$ to NH$_3$ equals 1:5, 1:10 and 1:20.

Despite methane and ammonia, we still need energy to generate
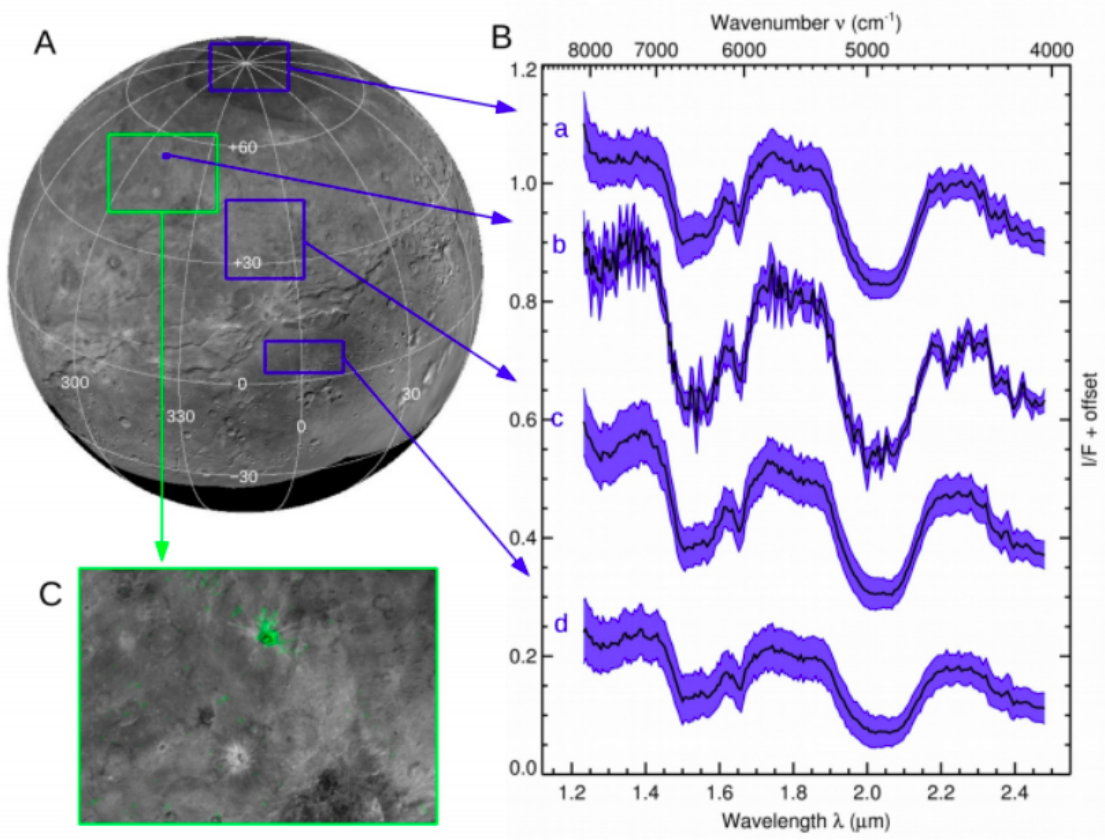
Figure 1.1: (A)The 2.2μm absorption taken by LEISA camera colored as green on the topology shown by LORRI camera and (B) the spectra at 4 positions with b taken near Organa crater.(quoted from [?])
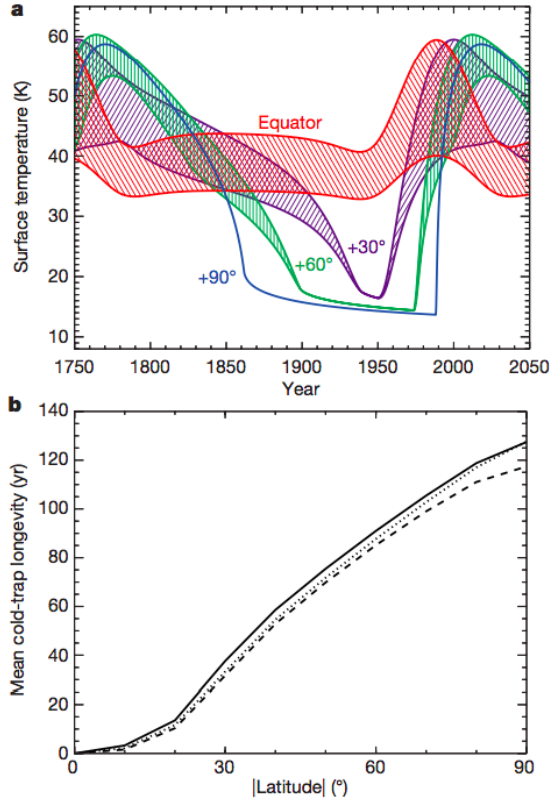
Figure 1.2: (a)The temperature of Charon with thermal inertia 10 J m^{-2} K^{-1} s$^{-1/2}$ in 1750 to 2050 Earth years and (b) length of time the latitude is under 25 K with the model averaged for 3 Myr with 2.5 (solid) 10 (dotted) and 40 (dashed) J m^{-2} K^{-1} s$^{-1/2}$.(quoted from [?])

CN$^-$. In our solar system, there are many energetic sources, including solar wind, photons, cosmic rays from the outer solar system, etc. Among these, Ly-α photons appears to be the most important source in the dark side of Charon. **It is attributed from resonance scattering by atomic hydrogen flow (the excitment of electrons by hydrogen atoms and release ly-α photons in all directions) in the solar system [?].** Its flux is 3.5×10^7 photons cm^{-2} s^{-1} at the winter pole of Charon [?] which is 50 % larger than expected before Mission New Horizons [?]. We perform VUV irradiation on CH$_4$+NH$_3$ experiments with different ratios (including 3:2, 1:5, 1:10 and 1:20) to simulate the photon induced evolution on different concentrations of CH$_4$. The ratios in previous studies with electron irradiation experiments are CH$_4$ to NH$_3$ equals 3:1[?] and 3:2[?]. As a complete study, we decided performing a ratio of CH$_4$ to NH$_3$ equals 3:2 to make possible comparisons.

4

Apart from VUV irradiation, EUV irradiation also irradiates on Charon. The direct EUV irradiation (>12.4 eV) is 8.7×10^7 eV cm^{-2} s^{-1} at mean heliocentric distance 39 A.U. whereas VUV irradiation (Ly-α photons) is 1.9×10^9 eV cm^{-2} s^{-1} calculated by Grundy et al. (2016)[**?**]. In order to investigate the effectiveness of EUV to VUV irradiation, we keep temperature of CH_4+NH_3 (3:2 & 1:5) ice mixtures at 15 K and use the monochromatic 30.4 nm (40.8 eV) ,He II light provided by High flux beamline at National Synchrotron Radiation Research Centre (NSRRC) in Taiwan to irradiate the ice mixtures. The relative ratios of EUV irradiated ice is CH_4 to NH_3 = 3:2 and 1:5 for possible comparisons with VUV irradiations.

In this text, we will introduce the experimental methodology in chapter 2, the formation mechanisms of main products of EUV and VUV irradiated CH_4+NH_3 ice mixtures in chapter 3. With these results, we will know more details of Charon, especially the influences of photon sources. Different energy sources including electron irradiation experiments , EUV and VUV irradiations, and their astrophysical implications will be presented in chapter 4.

2. Methods

2.1 Laboratory Astrophysics

To study the chemical reactivities in astrophysical environments (surface of Charon during winter time) experimentally, we conduct our experiments in Interstellar photoprocessing system (IPS) [?], an ultra-high vacuum chamber with base pressure 3×10^{-10} torr. By ideal gas law, the pressure corresponded to a density of 2×10^8 molecules cm^{-3}. We would like to particularly simulate the surface of Charon. The surface pressure of Charon is however not specific to high VU cross-section gases are not well defined yet, which will be in a future report by New horizons team, while all known species in Pluto's atmosphere to be below 0.3 nano bars (2.25×10^{-7} torr) [?]. The system will be introduced in detail in section 2.1.1. To simulate the irradiation in interstellar environments, we use a micro-wave discharge hydrogen lamp (MDHL) and monochromatic extreme-ultraviolet irradiation (EUV) 30.4 nm (40.8 eV)to irradiate our ice mixtures, and these will be introduced in section 2.1.2 and 2.1.3 respectively. The experimental protocols will be elaborated in section 2.2. For some non-physics background readers, basic theories of infrared spectroscopy and basic chemical kinetics used in data analysis are included in section 2.3 and 2.4 respectively.

2.1.1 Experimental simulations by IPS system

We conduct our astrophysical simulations in Interstellar Photo Processing System (IPS) (figure 2.1). IPS consists of three systems: the main chamber, where our experiments take places; the detection system, where we collect our data; and a gasline system, where we prepare our samples.

The main system consists of an ultrahigh vacuum chamber equips
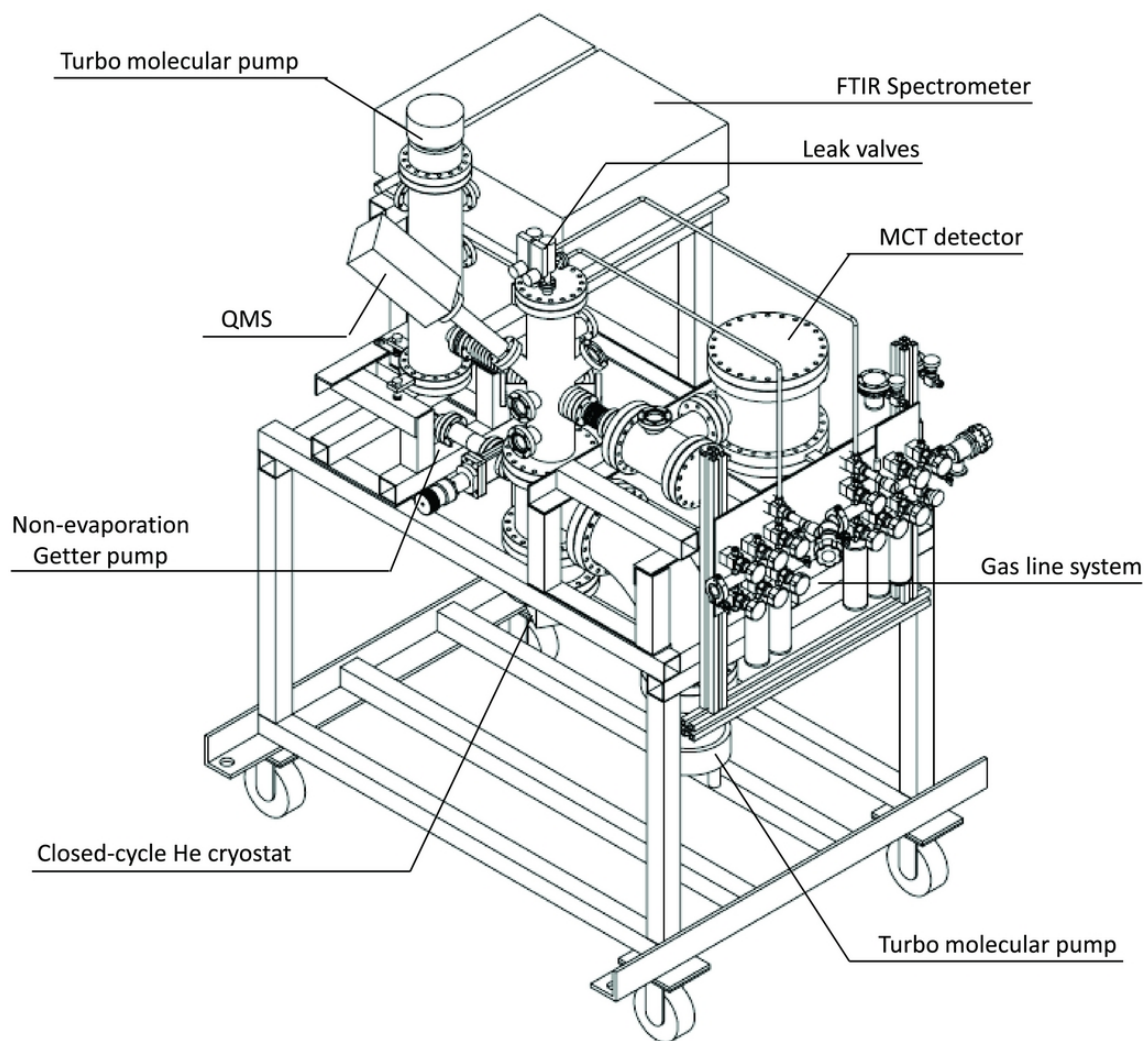
Figure 2.1: The schematic diagram of IPS system, mechanical pumps are not shown for clarity. (Quoted from Chen et al. 2014)

with a closed-cycle helium cryostat (CTI-M350). It is pumped by a turbo molecular pump, which is backed up by a scroll pump, and a non–evaporation getter pump. The getter pump, with a larger surface area, is a powerful tool to adsorb residue gases (H_2, CO and N_2) inside the main chamber, which can obtain a better base pressure. After baking, the base pressure of our main chamber can reach 1×10^{-10} torr at 15 K, monitored by a Granville-Phillips 370 Stabil-Ion gauge. This pressure can be used to simulate the dense cloud interior environments and star forming region. The substrate we have chosen is KBr, which is transparent to infra-red photons with 700 to 4000 cm^{-1}. It is mounted by substrate holder(oxygen-free copper), on the second stage of cold finger, which is on the tip of cryostat. A silicon diode and a heater are placed onto the cold finger, and another silicon diode is placed on the substrate holder. They are connected to a **LakeShore 331 temperature controller aquired PID (proportional–integral–derivative controller) system to achieve a warmup rate of 1K/min with an accuracy of 0.1 K.**

The detection system consists of a mid-infrared Fourier transform spectrometer (mid-FTIR) (ABB FTLA2000-104) and a Quadrupole Mass Spectrometer (QMS). To prevent absorption bands of CO, CO_2 and H_2O gas from the atmosphere, the IR beam path is built inside vacuum, pumped by dry pump. In this study, the infrared spectra are obtained with resolution of 4 cm^{-1} and averaged over 32 scans. The angle between the IR beam path and the substrate holder is 45 degrees. The QMS (MKS Microvision 2) consists of a controller and mechanical part sealed by a mounting flange in ultrahigh vacuum. It is mounted 10 cm from the substrate and runs with a resolution 0.5 a.m.u. The ionizer releases 70 eV electron by filament and ionizes incoming molecules to positive charged ions between anode grid and repeller. The ions are accelerated by focus plate and enters ion filter, which consists of four circular rods, with a combination of A.C and D.C. potential to sieve whole bandpass ions at millisecond timescale. The selected ions enter ion detector and are detected by either faraday cup and continuous dynode electron multiplier (CDEM) which can multiply weak signals.

The samples are prepared in situ in our gasline system. It contains four stainless steel bottles with the same volume, which is used to determine relative proportion of the gas mixtures by their partial pressures. The ammonia gas **(99.99%)** and methane gas **(99.999%)** are mixed with partial pressure measured by a Baratron (0 - 100 torr) with a 0.25% accuracy. The background pressure of the gasline system is lower than 1×10^{-7} torr, thanks to a turbomolecular pump (Oerlikon Leybold TurboVac 151, capacity 145 liters s^{-1}). It is backed up with a mechanical pump (Alcatel 2012A, capacity 450 liters minute^{-1}), equipped with an oil trap (molecular sieve type 13X).

2.1.2 Vacuum-UV source

In order to simulate the photoprocessing of vacuum ultraviolet (VUV) irradiation of the resonance scattered ly-α on surface of Charon during winter time, the ice mixtures are irradiated with a T-type Microwave-Discharged Hydrogen-flow lamp (MDHL). The middle part of the T-type quartz tube is being tunned by a ceramic rod that is called Evenson cavity. The molecular hydrogen with pressure 0.4 torr flows through the lamp with a support of a mechanical pump. Using a microwave generator and high voltage discharge, a low pressure plasma is produced in the Evenson cavity.

In order to measure the photon flux in situ, we use an 88 % transmittance nickel mesh with its photoelectric efficiency being obtained by high-flux beamline in National Synchrotron and a SXUV 100 photodiode calibrated by NIST. **A MgF$_2$ window is placed between the lamp and the main chamber to prevent hydrogen gas flow into the chamber.** Figure 2.2 shows a VUV emission spectrum of a MDHL with a cut off at 114 nm. It consists of Ly-α (121.6 nm) photons and H$_2$ molecular emission in the range of 110-180 nm. Chen et al. (2014)[**?**] showed that the spectral characteristics of the VUV light emitted in this range depends on the gas type (mixture of H$_2$ with He or Ar etc), pressure of H$_2$ and lamp geometry [**?**]. Throughout those configurations stated there, we adopted 0.4 torr molecular hydrogen and T-type MDHL that produces VUV irradiation at 114-170 nm with 19.1 % of Ly-α photons and a mean photon energy of 9.27 eV. The photon flux is 6.4 $\times$
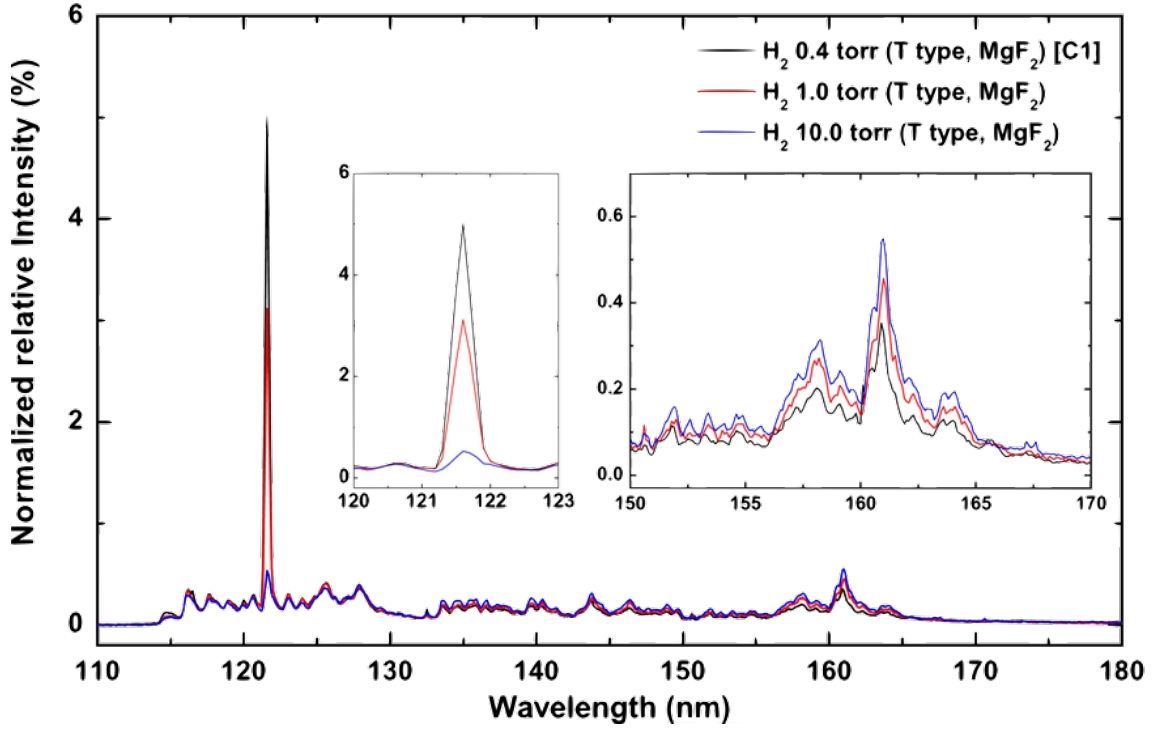
Figure 2.2: VUV spectra of MDHL (T-type geometry, 110-180 nm) with different H_2 pressure inside the lamp(Quoted from Chen et al. (2014)[?]) .

10^{13} photons cm^{-2} s^{-1} at sample position.

2.1.3   Extreme UV source

To simulate the solar EUV irradiation on both Charon and interstellar ices, we use the HF-CGM high – flux beam line of the National Synchrotron Radiation Research Center in Hsinchu, Taiwan. It provides a continuum EUV to VUV photons from 4 to 40 eV. The continuum is separated into monochromatic 30.4nm (40.8 eV)photons with a six-meter cylindrical grating monochromer with an incident angle of 70 degrees [?]. Similar to VUV irradiation provided by MDHL, the light intensity is monitored by the same nickel mesh with photoelectric efficiency obtained by SXUV 100 photodiode calibrated by NIST. With the known photoelectric efficiency, the flux of monochromatic 30.4nm (40.8 eV) is measured to be 2.15×10^{14} photons s^{-1} cm^{-2}, which is in the same order of magnitude of VUV continuum of MDHL. We replace the port with MDHL by the end station of the high-flux beamline. **A cryostat backed up by a scroll pump is placed between our system and the beamline endstation to adsorb water molecules**

from endstations during irradiation. Between the cryostat and our main chamber is a SiO$_2$ valve, which is shuted during the warm-up phase to maintain a similar warm-up environment in main chamber when we were using MDHL as irradiation source.

2.2   Experimental Protocol

In this section, we will briefly introduce the procedures of how we perform our experiments. It is divided into four parts, preparation and cooling, deposition, irradiation and warmup.

2.2.1   Preparation of experiments and cooling

Before any of experiment is done, we bake our system at 100 °C, for 48 hours to reduce the contamination of water and residue gases as much as possible. It is cooled to room temperature that the background pressure can reach routinely at 1×10^{-10} torr. The gasline is connected with the regulators of the gas tanks and bake to 100 °C and pumped by turbomolecular pump for two days before any experiments are done. Before cooling the substrate to cryogenic temperature, we take an infrared(IR) spectrum and start the monitoring of residue gases by QMS in order to compare the residue molecules and to verify any possible contaminations in the main chamber. We then start the cooling process with the help of the closed-cycle He cryostat.

2.2.2   Deposition

The gas mixtures are pre-mixed in our gasline system introduced in section 2.1.1. We control the relative proportion of two ice mixtures by sealing corresponding partial pressure gases in two equal volumn stainless steel bottles. We condense the gas premixed in the stainless steel bottles onto pre-cooled KBr substrate via leak valve. The substrate is monitored by Fourier-Transform Infrared (FTIR) Spectrometer and Quadrupole mass spectrometer (QMS) during deposition. The pressure of deposition is fixed to 1×10^{-8} torr that the deposition rate is around 4×10^{16} molecules cm^{-2} min^{-1}, which varies in different relative ratio of our ice mixtures because the differences in sticking coefficients. After

deposition, we place the ice mixture at 15 K for 60 minutes and allow pumping of residue gases, until the pressure of the main chamber falls back to its base pressure to simulate the interstellar environment before any irradiation.

2.2.3 Photon Irradiation

The total irradiation time is 270 minutes (with some 450 minutes, depend on experiment configurations) with time intervals varies from 2 to 30 minutes. After each irradiation, we wait for 10 minutes allowing pumping out of the photodesorbed gas molecules. During irradiation, the photon flux is monitored by a nickel mesh. After Irradiation, we place the sample for 30 minutes in case if any further reaction is processed.

2.2.4 Warmup

We heat the tip of cold finger to 300 K (measured by silicon diode near the substrate) with rate 1 K/min. During warmup, we record the QMS from 1 to 100 a.m.u. to observe if there are low quantity of higher mass products formed during irradiation. Apart from QMS, we scan infrared spectra with 5 K intervals to monitor the evolution of infra-red active species such as photo products and reactants. With both infra-red and QMS, we may better identify the photo products by kinetic energy gained during warm-up and temperatures the desorpted.

2.3 Infra-red spectroscopy and the Beer-Lambert's Law

We use infra-red spectroscopy extensively in chapter 3. It is a powerful tool to study molecular interactions during irradiation and warmup. We choose infra-red rather than Raman spectroscopy because infra-red has lower energy that it would not change the structure of the ice mixture nor breaking any of the bonds. In addition, it is also much richer in terms of identifying functional groups especially when studying ice mixtures whose vibrational modes falls in the mid-IR wavelength ranges. With different vibrational modes, the energy absorbed by molecules are quantified. With the energy of absorption bands in infra-red spectrum, we may identify the functional group of the species. To simply clas-

sify, vibrational motions can be divided into stretching and bending. Stretching needs more energy than bending. For stretching, there are symmetric and asymmetric stretchings; while bending can be divided into in-plane (scissoring, rocking) and out-of-plane (wagging and twisting) (Figure 2.3).

By Beer's Law, we may calculate the column density of the molecule with its functional groups, which are used to plot figures in chapter 3 and 4. Beer Lambert's Law suggests that when light passes through a medium, the amount of light absorbed is proportional to density and path length of the medium. Assume a known intensity beam $I_0(\nu)$ passes through the medium and beam intensity become $I(\nu)$. The transmittance $T(\nu)$ is defined by equation 2.1.

$$T(\nu) = \frac{I(\nu)}{I_0(\nu)} \tag{2.1}$$

Also, the absorbance $a(\nu)$ is defined by equation 2.2.

$$a(\nu) = -\ln T(\nu) = -\ln \frac{I(\nu)}{I_0(\nu)} = nl\sigma(\nu) \tag{2.2}$$

where n is number density (molecules/cm^3), l is the path length (cm), $\sigma(\nu)$ is the cross-section (cm^2/molecule) of corresponding frequency ν. This equation is known as Lambert Beer's Law.

As the ice mixtures in our thesis are at 15 K, the peaks of absorbance are often a broadband due to coupling between neighbor molecules. Therefore, we can integrate the whole band of the peak by equation 2.2 with respect to frequency. Combines the (integrated) absorbance band strength (A value) in literatures to calculate the column densities N of the ices by equation 2.3.

$$N = \frac{\int a(\nu)\mathrm{d}\nu}{A(\nu)} \tag{2.3}$$

where N is the column density (molecule cm^{-2}), $A(\nu)$ is the absorbance strength (cm molecule^{-1}).

Symmetric stretching

Asymmetric stretching

In-plane Bending

In-plane Rocking

Out-of-plane Wagging

Out-of-plane Twisting

$+$ indicate motion out of the page

$-$ indicate motion into the page
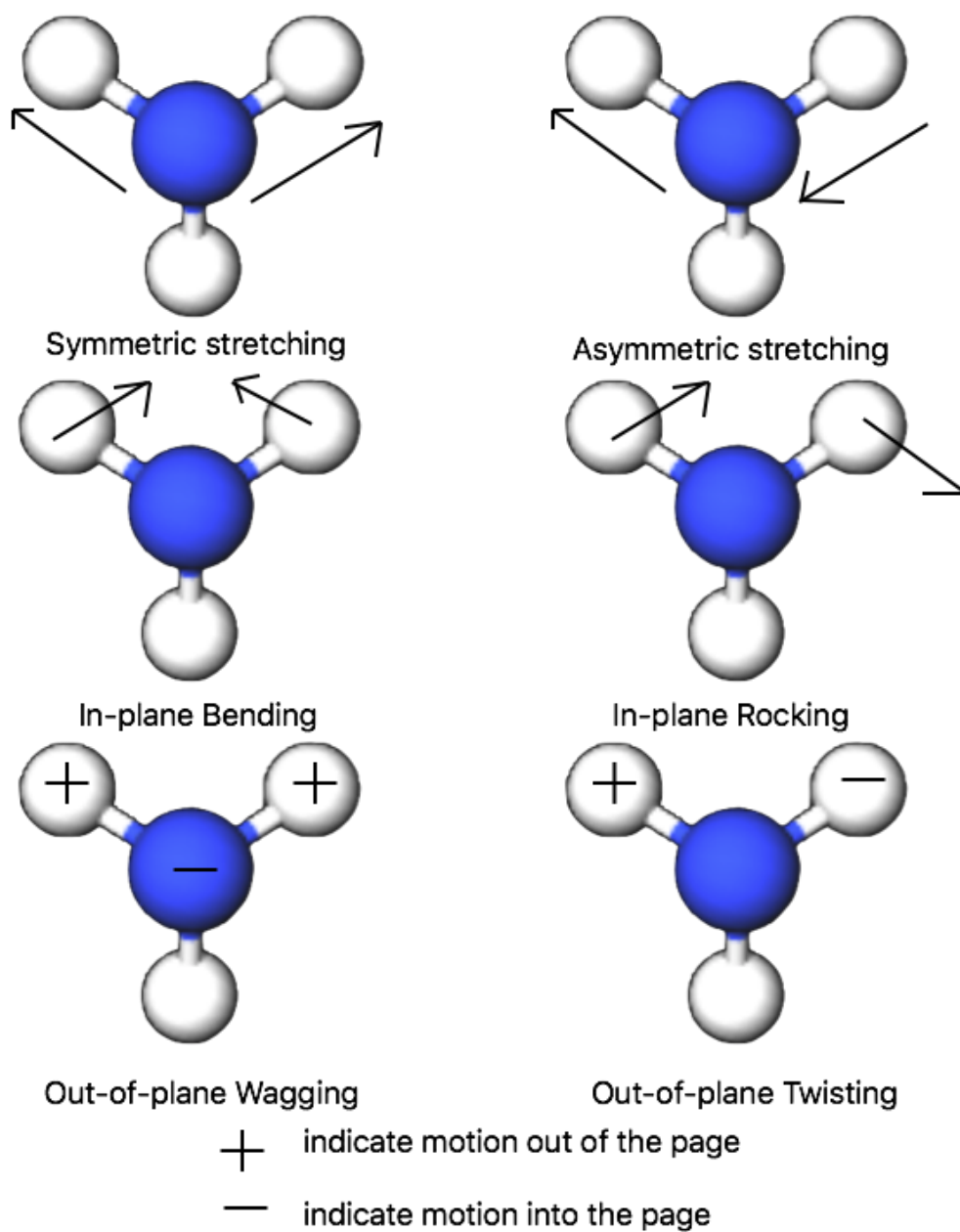
Figure 2.3: Different vibrational modes of a **NH$_3$ molecule**.

2.4 Reaction Rate Laws

In this section, we will introduce rate reaction of a consecutive reaction and the concept of pseudo first order which we use to fit our reaction product against photon dose in chapter 3. The rate of a chemical reaction is a change in concentration of a substance per unit of time.

To determine the order of a reaction, we can only determine it experimentally. For a zero order reaction, the rate $= -\frac{d[R]}{dt} = k[R]^0$. By calculus, $[R]_0 - [R]_t = kt$.

For a first order reaction, rate $= -\frac{d[R]}{dt} = k[R]$. By calculus, $\ln[R]_t = -kt + \ln[R]_0$.

For a second order reaction, rate $= -\frac{d[R]}{dt} = k[R]^2$. By calculus, $\frac{1}{[R]_t} - \frac{1}{[R]_0} = kt$.

In a reaction with one reactant in excess, the rate of reaction is called pseudo first order reaction where pseudo means pretended. For D+E $\rightarrow$ F, rate $= k[D][E]$. As $[E]_0 \gg [D]_0$, change of $[E]$ is negligible that $[E] \sim [E]_0$. Therefore, $[E]$ is assumed to be a constant and included in the rate constant k.

For a consecutive reaction equation, which we used to fit our data points, where D $\rightarrow$ E $\rightarrow$ F that the produced product will not convert back as reactant. A simple example is radioactive decay. At $t = 0$, $[D] = [D]_0$, $[E] = 0$, $[F] = 0$ and at all times, $[D] + [E] + [F] = [D]_0$. The rate equations are as follows:

$$\frac{d[D]}{dt} = -k_1[D] \tag{2.4}$$

$$\frac{d[E]}{dt} = k_1[D] - k_2[E] \tag{2.5}$$

$$\frac{d[F]}{dt} = k_2[E] \tag{2.6}$$

By equation 2.4, we get

$$[D] = [D]_0 e^{-k_1 t} \tag{2.7}$$

By substituting equation 2.7 into equation 2.5, we get

$$\frac{d[E]}{dt} + k_2[E] = k_1[D]_0 e^{-k_1 t} \tag{2.8}$$

After solving the differential equation 2.8 , we get

$$[E] = \frac{k_1}{k_2 - k_1}(e^{-k_1 t} - e^{-k_2 t})[D]_0 \tag{2.9}$$

Finally, since $[F] = [D]_0 - [E] - [D]$, by equation 2.7 and 2.9, we get

$$[F] = \left(1 + \frac{k_1 e^{-k_2 t} - k_2 e^{-k_1 t}}{k_2 - k_1}\right)[D]_0 \tag{2.10}$$

3. Results and Discussions

In this chapter, we will investigate the following mainly by infrared spectroscopy: 1. The photoproducts produced by different concentration ratios of methane to ammonia, 2. the reaction mechanisms of each main products, 3. the photo products produced by EUV and VUV photons and 4. the functional groups of tholin formed by irradiation of VUV, EUV on different relative proportions of CH_4:NH_3 ice mixtures (the result is compared with the residues on Titan produced by Imanaka et al. [?]).

3.1 The infrared spectra and peaks identification

Figure 3.1 is a typical infrared spectrum of CH_4:NH_3 ice mixtures in different concentration ratios: 1:20, 1:10, 1:5 and 3:2 where ammonia is fixed with a column density 6×10^{17} molecules cm^{-2}. We scan the IR spectrum prior to the irradiation at 15 K (for details of methodology, please refer to section 2.2).

Table 3.1: The strength of absorbance adopted in this thesis measured in literatures of pure ice samples

Wavenumber (cm^{-1})	Assignment	Vibration	FWHM	A value ($\times 10^{-17}$)	Reference
2976	C_2H_6	-CH_3	-	1.05	2
2960	C_3H_8	-CH_2-	-	2.58	2
2086	CN^-	CN	-	1.8	3
1297	CH_4	CH deformation	8	0.61	1
1070	NH_3	"umbrella mode"	68	1.7	1

Reference: 1. d'Hendecourt and Allamandola (1986)[?] 2. Moore and Hudson (1998)[?] 3. Noble et al. (2013) [?]

The peaks used in column density calculations (by equation 2.3) are labelled by dotted lines in the graph (figure3.1). We are aware that IR absorption strengths can vary depending on its environment, which means it will be different when it is pure, when it is mixed with other
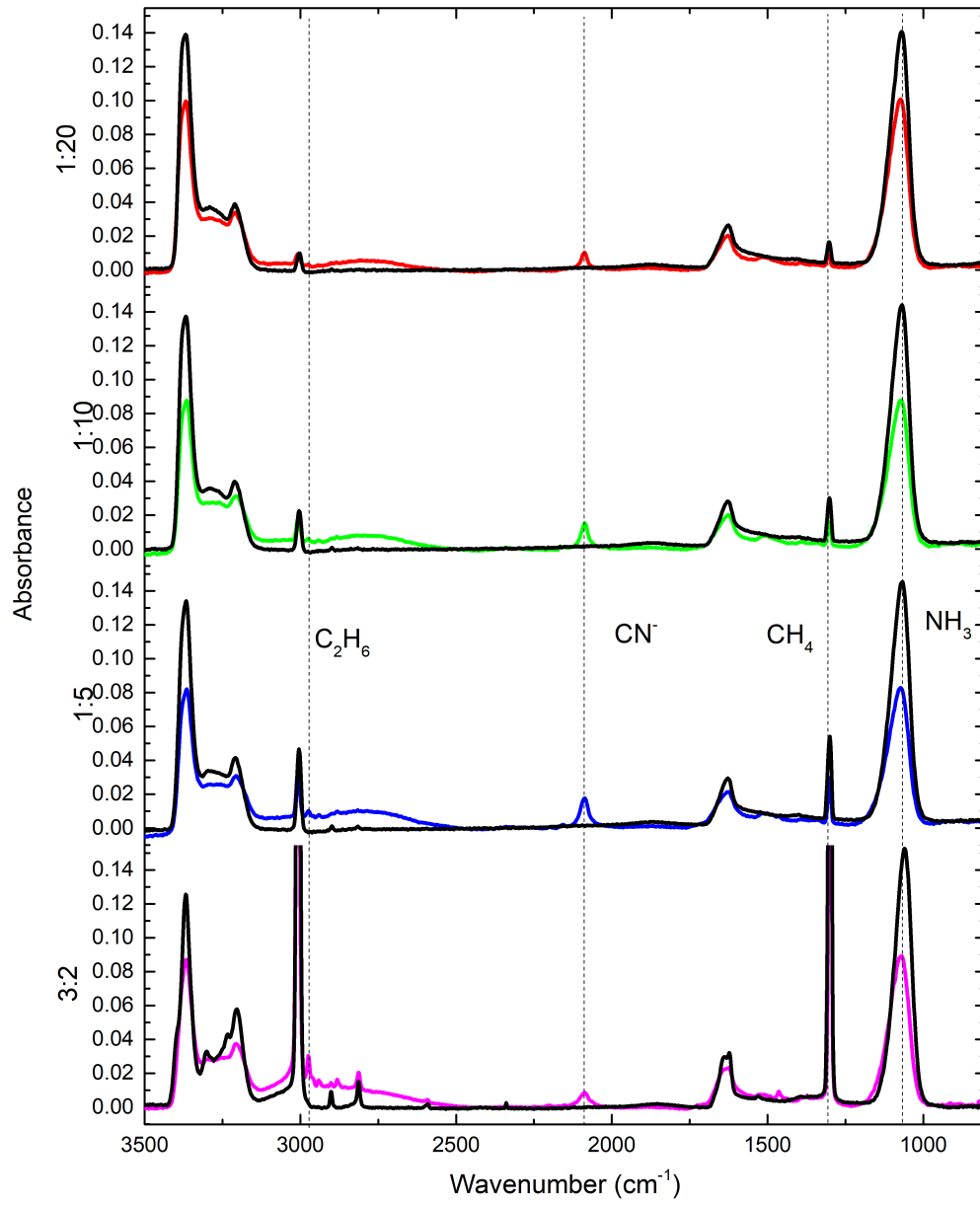
Figure 3.1: The the infrared spectrum of CH$_4$ + NH$_3$ ice mixtures before irradiation (black) and after VUV (MDHL) irradiated (coloured) ice mixtures.

ices, and will vary with the relative proportions between ice components. We are justified to use the same absorption strength throughout our discussion to estimate the column density of each species and how the absorption area changes with concentration ratios of ice mixtures and photon energy. The absorption strengths we adopted are stated in table 3.1

Figure 3.2 is a zoomed view of figure 3.1. Multiple peaks are used in product assignments, which are presented in table 3.2. The absorption peak located at 2975 cm^{-1} corresponds to the strongest vibration of C_2H_6.

The peak positioned at 2960 cm^{-1} belongs to -CH_2- so we tentatively assign that as C_3H_8, which is the shortest carbon chain molecule contains -CH_2-. By fitting the peaks as a few gaussians, we deconvolute the overlapped C_2H_6 and C_3H_8 into two gaussians. The signal$-$to$-$noise ratio in CH_4:NH_3 = 1:10 is poor that we can not quantify the amount of C_3H_8 (figure 3.2).

Figure 3.3 is zoomed infrared absorption spectra of CN^-. We assign the peak 2086 cm^{-1} to CN^- but not a combination of HCN and CN^-. The assignment is based on a absence in CN bending mode at 848 cm^{-1}. In the case CH_4 + NH_3 = 3:2,a peak located at 820 cm^{-1} is observed, the charateristic of the band is different from HCN (halved FWHM of HCN) and it is eliminated at 50 K during the warm-up phase. Since 50 K is the desorbing temperature of C_2H_6 and the peak position is close to ν12 mode of C_2H_6, we believe that the 820 cm^{-1} peak is contributed by C_2H_6. Therefore, peak located at 2086 cm^{-1} is assigned as purely CN^-. After identification of the main products (C_2H_6, CN^- and C_3H_8), we will look into the mechanisms one by one in the next section.
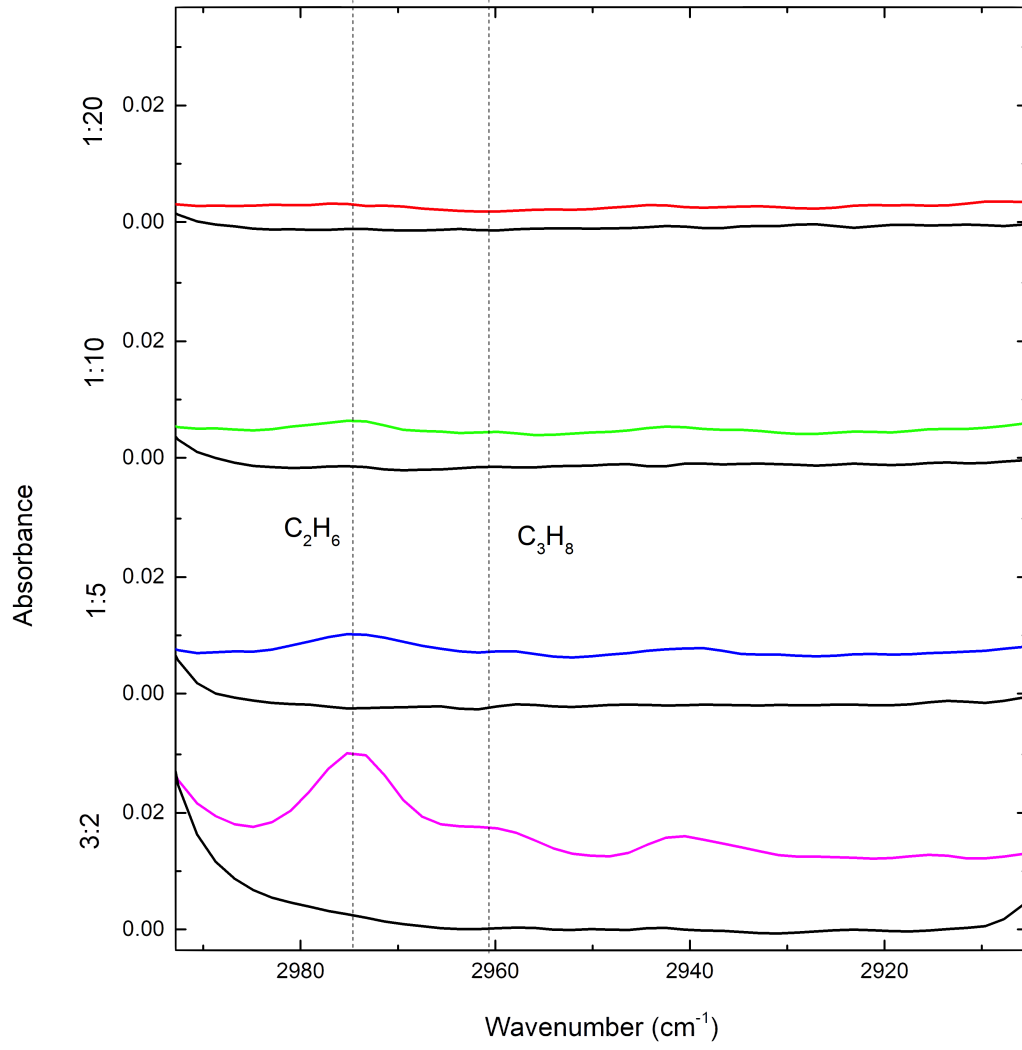
Figure 3.2: The infrared spectra of CH_4 + NH_3 ice mixtures in the range of C_2H_6 and C_3H_8 vibrations before irradiation (black) and VUV irradiated ice mixtures provided by MDHL.
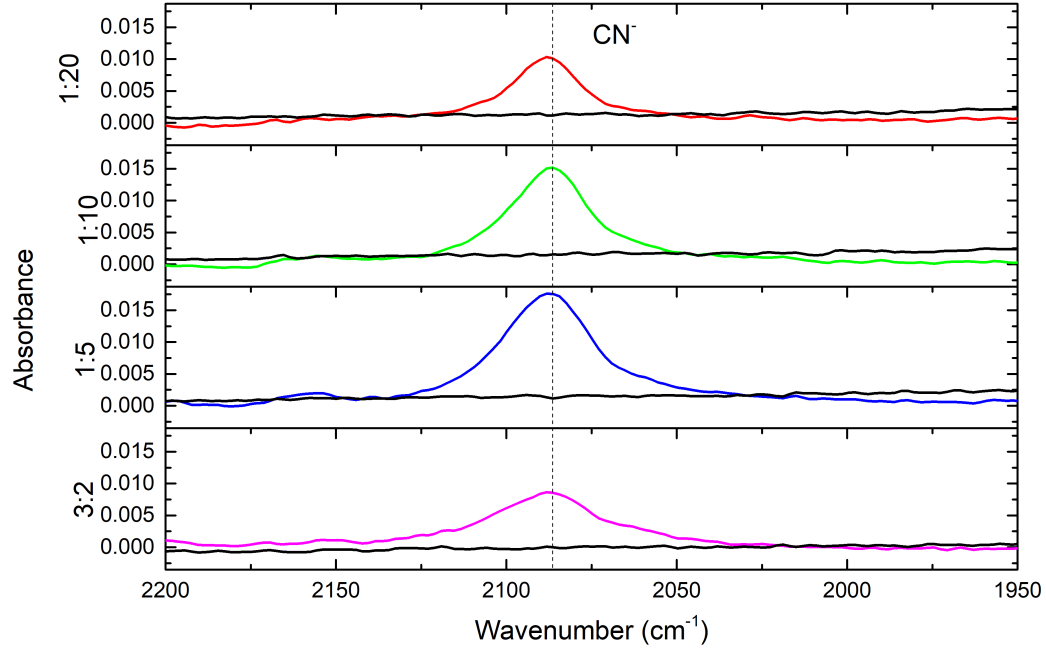
Figure 3.3: The infrared spectra of $CH_4 + NH_3$ ice mixtures in the range of CN^- before irradiation (black) and VUV irradiated ice mixtures provided by MDHL.

Table 3.2: The peak positions of identified substances after irradiation in different relative proportions of ice mixtures.

Literture assignments		CH$_4$:NH$_3$ ratio (MDHL)				
Wavenumber (cm^{-1})	Identified IR modes	1:5 (cm^{-1})	1:10 (cm^{-1})	1:20 (cm^{-1})	3:2 (cm^{-1})	Ref.
3375	ν_3 (NH$_3$)	3366	3366	3369	3367	1
3210	ν_1 (NH$_3$)	3207	3208	3210	3205	1
2972	ν_{10} (C$_2$H$_6$)	2975	-	-	2975	3
2960	C$_3$H$_8$	-	-	-	2960	7
2941	$\nu_8 + \nu_11$ (C$_2$H$_6$)	2940	-	-	2940	3
2904	ν_1 (CH$_4$)	2901	-	-	2901	5
2879	ν_5 (C$_2$H$_6$)	2882	2883	-	2882	3
2814	$\nu_2 + \nu_4$ (CH$_4$)	-	-	-	2815	5
2083	ν (CN$^-$)	2088	2087	2088	2088	2
1625	ν_4 (NH$_3$)	1625	1625	1626	1631	1
1514	δ (NH$_2$)	1509	1507	1505	1511	6
1465-1440	deform CH$_2$ scissor	1461	-	-	1463	3,4
1390-1370	CH$_3$ sym deform	1394	1394	1394	1372	4
1298	ν_4 (CH$_4$)	1301	1302	1305	1299	2
1075	ν_2 (NH$_3$)	1073	1072	1072	1072	1
820	ν_{12} (C$_2$H$_6$)	-	-	-	820	3

Reference: 1. Bossa et al. 2008 [?] 2. Moore and Hudson 2003 [?] 3. Kim et al. 2010 [?] 4. Socrates 2001 [?] 5. Bennet and Kaiser 2007 [?] 6. Zheng et al. 2008 [?] 7. Hudson and Moore 2004 [?]

3.2 Reaction mechanisms and fitting results

3.2.1 C_2H_6

The formation of C_2H_6 in astrophysical environment is mainly a combination with 2 CH_3 radicals [?]:

$$CH_4 + h\nu \rightarrow CH_3 \tag{3.1}$$

$$2CH_3 \rightarrow C_2H_6 \tag{3.2}$$

The energy requires to break the CH bond of CH_4 is **4.43 eV[?].** **From Bennet et al. (2006)[?],the recombination of 2 CH_3 radicals forms a internally excited C_2H_6, and releases 3.74 eV to the surrounding matrics or decompose unimolecularly to become ethly radicals (C_2H_5) or ethene (C_2H_4) (required extra of 0.53[?] and 0.84 eV[?] respectively).** Therefore, the process in equation 3.2 is a no-barrier exothermic process. The formed C_2H_6 is internally excited that it is able to become C_2H_4 etc. Figure 3.4 depicts the formation column density as a function of irradiation time of C_2H_6 in different relative proportions of irradiated ice mixtures. As the formation only depends on CH_4, first order kinetics equation is adopted to fit the column density versus photon dose.

$$[C_2H_6] = B(1 - e^{-kt}) \tag{3.3}$$

Where B is the column density of C_2H_6 achieved when irradiated for infinitly long. The fitting results are shown in table 3.3. From table 3.3, the production rate is nearly proportional to the initial CH_4 concentrations. Note that C_2H_6 is not detected in CH_4 to NH_3 = 1:20 ice mixtures.

Table 3.3: The fitting results of C_2H_6 by $[C_2H_6]=B(1 - e^{-kt})$

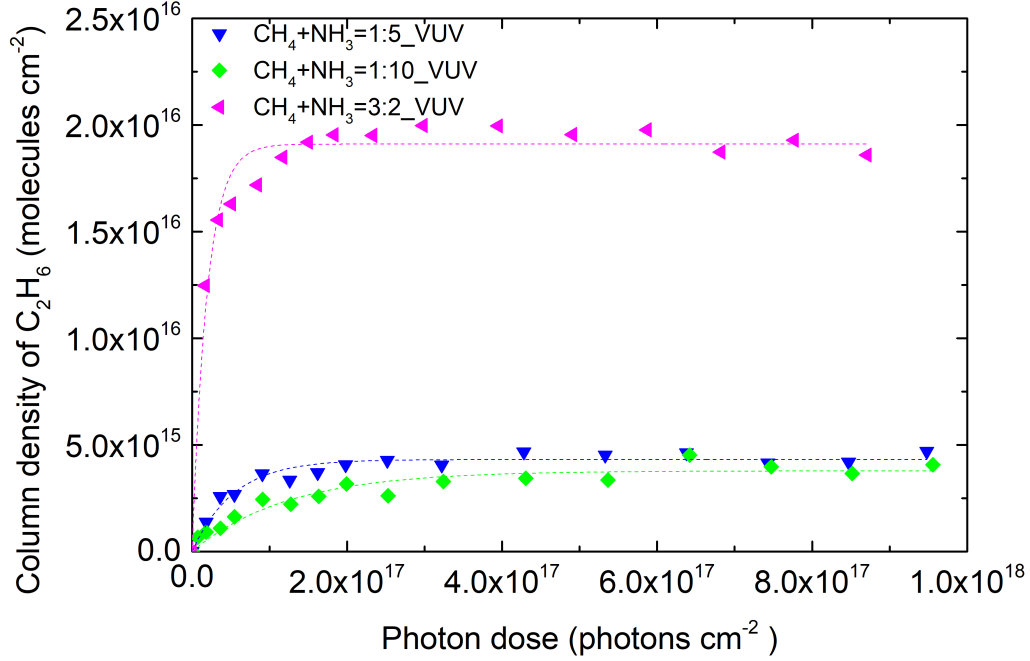| Ratio of CH_4:NH_3	$[C_2H_6]_o$ (x10^{15} molecules cm^{-2})	k (x10^{-17} photon^{-1})
1:10	2.90 ± 1.25	0.92 ± 0.15
1:5	4.16 ± 0.28	2.28 ± 0.28
3:2	19.2 ± 0.15	5.28 ± 0.25

Figure 3.4: The column density of C_2H_6 during $CH_4 + NH_3$ ice mixtures irradiated by MDHL.

3.2.2 C_3H_8

Propane is a secondary product formed by a combination of either $C_2H_6 + CH_2$ (equation 3.4)or $C_2H_4 + CH_4$ (equation 3.5). From Bennet et al. (2006) [?], C_2H_4 is decomposed by the internally excited C_2H_6. With subsequently impinging electrons, it is degraded into C_2H_3 and C_2H_2 with an energy barrier of 4.69 and 4.06 eV respectively.

$$C_2H_6 + CH_2 \rightarrow C_3H_8 \tag{3.4}$$

$$C_2H_4 + CH_4 \rightarrow C_3H_8 \tag{3.5}$$

Table 3.4: The fitting results of C_3H_8 by $\mathbf{[C_3H_8]}{=}C(1 - e^{-k_1 t})$

Ratio of CH_4:NH_3	A (x10^{15} molecules cm^{-2})	k (x10^{-17} photon^{-1})
1:5	0.46 ± 0.17	2.89 ± 2.44
3:2	3.84 ± 0.18	2.08 ± 0.18

Note that this peak (2960 cm^{-1}) is only tentative assignment which consists of mainly C_3H_8, other species such as C_2H_6 and carbon chains with -CH_2- also contributes to the peak. C **is similar to** B **that it is the column density of** C_3H_8 **after infinitly long irradiation time.**

The column densities are shown in figure 3.5, where the fitting results are shown in table 3.4. Since the C_3H_8 detection in $CH_4 + NH_3$
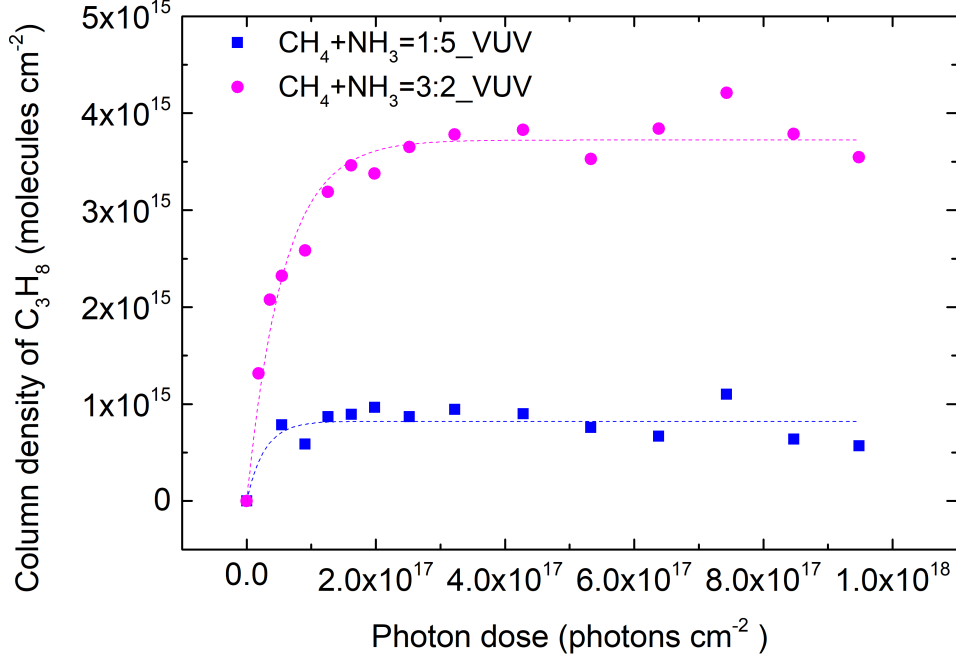
Figure 3.5: The column density of C_3H_8 during CH_4 + NH_3 ice mixtures irradiated by MDHL.

= 1:5 ice mixtures are close to our detection limits, the errors of the fitting results would attributes to a meaningless fitting.

3.2.3 CN^-

The formation mechanism of CN^- at low temperature was suggested by Kim and Kaiser (2011) to be two step reaction mechanism with methylamine as intermediate[?]. CH_4 and NH_3 irradiated by photon become CH_3 and NH_2 radicals, followed by propagation and recombination of radicals becoming CH_3NH_2 and dehydrogenation and acid-base reaction to form CN^- (figure 3.6).

Kim and Kaiser (2011) used 1.5 keV electron as energy source to simulate the cosmic ray induced photochemistry [?]. Despite the extra heats generated in these exothermal reactions**(calculated by Kundu et al.(2017)[?])**:

$$CH_2 + NH_3 \rightarrow CH_3NH_2, \Delta H = -3.7eV \qquad (3.6)$$

$$CH_4 + NH \rightarrow CH_3NH_2, \Delta H = -3.14eV \qquad (3.7)$$

$$CH_3 + NH_2 \rightarrow CH_3NH_2, \Delta H = -3.64eV \qquad (3.8)$$

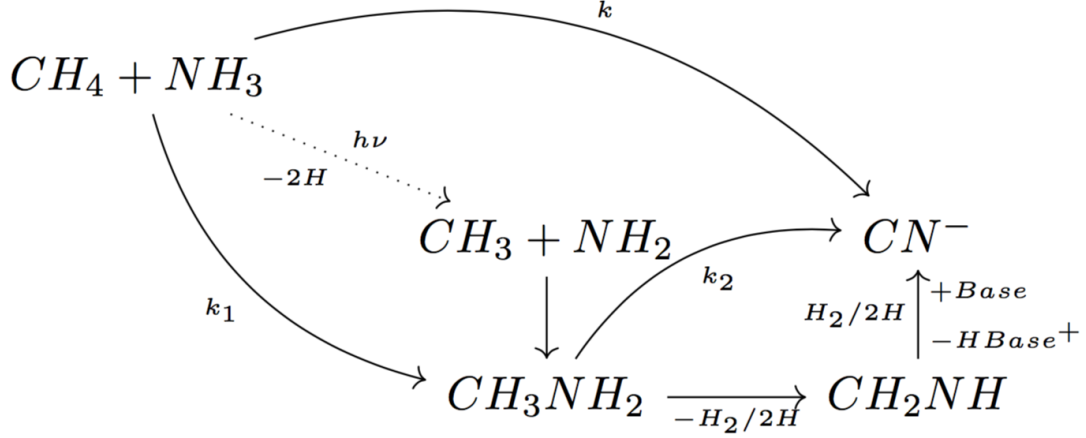$$CH_4 + NH_3$$

Figure 3.6: The formation mechanism of CN^- proposed by Kim and Kaiser(2011)[?], we denote the one step mechanism with rate constant k, and two step pathway by k_1 and k_2;**the value of** k equals k_1 when $k_2 \gg k_1$.

Kundu et al. (2017) [?] fails to observe methylamine as intermediate during warmup phase after using $1-90$ eV electrons to initiate CH_4 and NH_3 ice mixtures. **They explained that the non-detection is due to their thin ice thicknesses (6-7 ML and 3-4 ML for CH_4 and NH_3 respectively). The small beam size (4 mm^2) and fast heating rate (60 K/min) are also contributing factors. With the small amount of the processed ice in such a small area, combining the slow sampling rate in QMS (about 2 points per second), it is not a surprise for the non-detection.** This formation mechanism also applies in our photon irradiation experiments because we can also detect the methylamine during our warm-up phase. **The ion fragment with m/z=31 is assigned as $CH_3NH_2^+$ including the m/z=30 corresponding to CH_3NH and CH_2NH_2 are detectable in all ratios of our $CH_4 + NH_3$ experiments at 120 to 150 K (figure 3.7).**

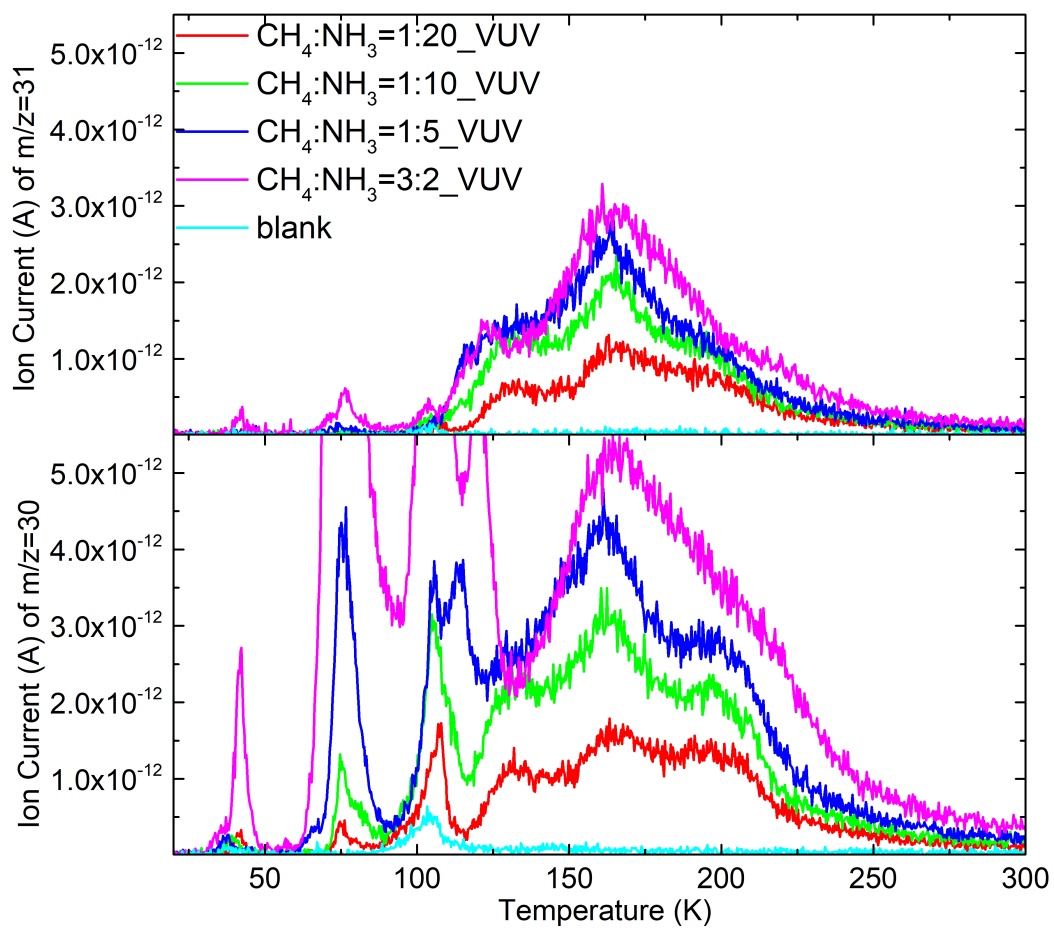Mentioned in section 2.4, we use rate equation for consecutive reac-

Figure 3.7: The ion current with mass to charge ratio **31 and 30** detected by QMS during warm-up with heating rate 1 K/min in different relative proportions of ice mixtures.

tions 2.10 to fit our CN^- column densities. This rate equation applies in our experiments with one of the reactants in excess. **Although CH_4 is more abundant than NH_3 (CH_4:NH_3=3:2), their comparable concentrations still tends to a second order kinetics.** Contrastly, NH_3 is in excess (CH_4:NH_3 = 1:5, 1:10 and 1:20), the pseudo first order assumption applies. Throughout the formation mechanism, one of the reactants (neither C or N) is a limiting reactant, therefore, the rate equation 2.10 is adopted to fit the formation of CN^- (figure 3.8). **The same equation was adopted to fit the CN^- from in CH_4:NH_3=3:2 ice mixtures in order to make comparison with the other configurations/**

The fitting results are averaged by **several** experiments and are shown in table 3.5. We find that one of the rate constant is always larger than the other in all of the ratios. The results of Kim and Kaiser (2011) is also listed into the table, they could observe a two-step reaction mechanism in production of CN^- in CH_4:NH_3 =3:1 experiments with electron current 0.1 μA. However, when they increase the electron flux to 1 μA for irradiating C_nH_{2n+2} (n=1-6) and NH_3 ice mixtures, they observed a one-step reaction mechanism [?].

Table 3.5: The fitting results of CN^- by equation 2.10

Ratio	A (x10^{16} molecules cm^{-2})	k$_1$ (x10^{-18} photon^{-1})	k$_2$ (photon^{-1})
	VUV experiments with CH_4:NH_3 ice mixtures		
1:20	4.75 ± 0.40	0.70 ± 0.09	»1
1:10	4.51 ± 0.18	1.33 ± 0.13	»1
1:5	4.61 ± 0.18	1.93 ± 0.19	»1
3:2	2.24 ± 0.03	8.21 ± 0.70	»1
	Quoted from Kim and Kaiser[?]		
Ratio	[CN^-](x10^{16} molecules cm^{-2})	k_1 ($\times 10^{-3}$ s^{-1})	k_2 ($\times 10^{-3}$ s^{-1})
	0.1 μA e$^-$ with CH_4:NH_3 ice mixtures		
3:1	1.3 ± 0.0	2.7 ± 0.3	8.9 ± 1.6
	1 μA e$^-$ with C_nH_{2n+2} (n=1-6)+NH_3 ice mixtures		
2:5	1.0 ± 0.0	8.7 ± 1.3	»1

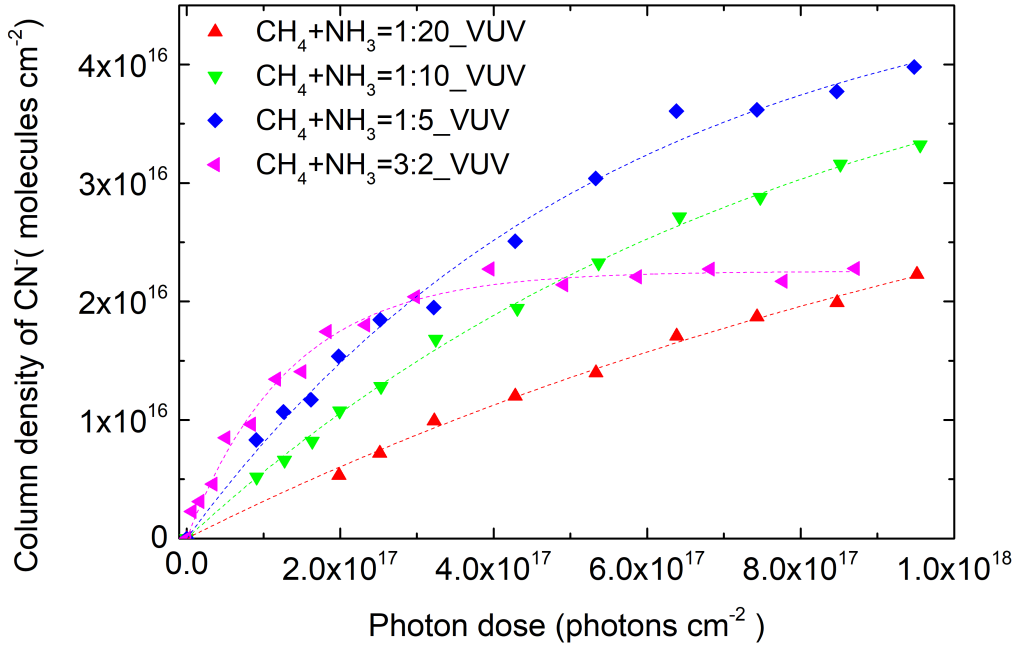The second column represents the column density of CN^- obtained when irradiated the ice for infinitely long.

Figure 3.8: The column density of CN⁻ accumulated when different relative proportions of CH_4 + NH_3 ice mixtures are irradiated by VUV photons provided by MDHL. The dotted lines are fits of column densities by equation 2.10.

3.3 The Concentration Effects in CN⁻formation and the relation with C_2H_6 and C_3H_8

3.3.1 Cyanide ion and Ethane

From table 3.5, the rate k_1 is nearly proportional to the concentration of CH_4. As CH_4 to NH_3 ratio increases in ammonia dominated ices, more CH_4 are involved in CH_3 radical formation, thus there are more CH_3 radicals to produce CH_3NH_2 intermediates(figure 3.9).

In CH_4 to NH_3 =3:2 ice mixtures, however, the cyanide ion formed is about half of that of the other ratios. The decrease is mainly because NH_2 (forming CH_3NH_2) has a competing relationship with CH_2, CH_3 and C_2H_4 radicals (forming C_2H_6 and C_3H_8). This competition supresses the production of intermediate CH_3NH_2, thus the formation of CN⁻ (figure 3.10). Therefore, the yield of CN⁻ is the least in CH_4 to NH_3 ice mixture with ratio 3:2 while the yield of C_2H_6 is the greatest in the mixture with the same ratio(table 3.5 and 3.3). Figure of CN⁻ and

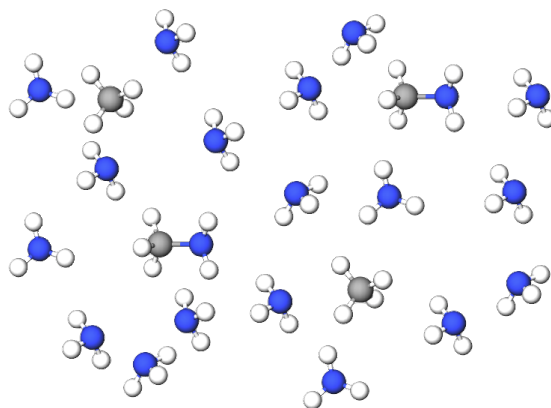Figure 3.9: The NH_3 in excess situation where increasing CH_4 concentrations enhances the production of CN^-. The blue balls indicate N atoms, white balls indicate H atoms while grey balls are C atom.
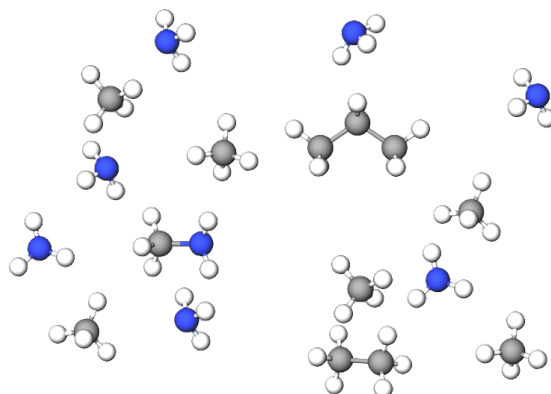

Figure 3.10: The CH_4 in excess situation where CH_4 reacts with neighbouring CH_4 molecules producing C_2H_6 and C_3H_8. The blue balls indicate N atoms, white balls indicate H atoms while grey balls are C atoms.

C_2H_6 (figure 3.11) shows the formation of CN^- in ice mixtures with diluted CH_4 has more CN^- formed than C_2H_6. It is because ice mixtures with higher concentrations in CH_4 is more effective for one CH_3 radical to combine with another CH_3 radical. In contrast, CH_3 radicals formed in the ice mixtures with diluted CH_4 concentrations are aggregated by NH_3. Therefore, CN^- is more efficient to form in ice mixtures with excess NH_3.

The formation rate of CN^- in CH_4:NH_3 = 3:2 ice mixtures is highest because they have similar photon dose. The absorption cross-section in the range of 120 - 175 nm by NH_3 is 1-2 $\times$ 10^{-17} cm^2 measured by Cruz-Diaz et al. (2014)[?], while CH_4 is measured to be 1.5 $\times$ 10^{-17} cm^2 at ly-α region and 0.1 $\times$ 10^{-17} cm^2 at molecular hydrogen emition regions measured by same group[?]. Mentioned at chapter 2, 19.1% of photons emitted by our MDHL is ly-α. It is therefore expected that the two species receives similar amount of photon dose when their relative ratio is CH_4:NH_3 = 3:2. With this similar photon dose, assuming their formation rate of CH_3 and NH_2 radicals are similar, the concentration of the two radicals in the ice mixtures are similar. Similar amount of CH_3 radical and NH_2 radicals can form CH_3NH_2 much easier than CH_4 surrounded by 5 NH_2 radicals. Therefore, a higher production rate of forming CN^- is achieved.

3.4   Photon Energy Effect - EUV and VUV

According to Blanksby and Ellison (2003), the dissociation energy for CH_4, becoming CH_3, CH_2, CH and C are 4.55, 4.79, 4.39 and 3.51 eV respectively at 298 K; whereas dissociation energy for NH_3, becoming NH_2 is 4.67 eV at 298 K[?]. Considering our MDHL with average energy of 9.27 eV, the photon energy is enough for all of the above fragmentation pathways. Although increasing the photon energy does not create new fragmentation pathway, the choice of fragmentation pathways depends on photon energy.
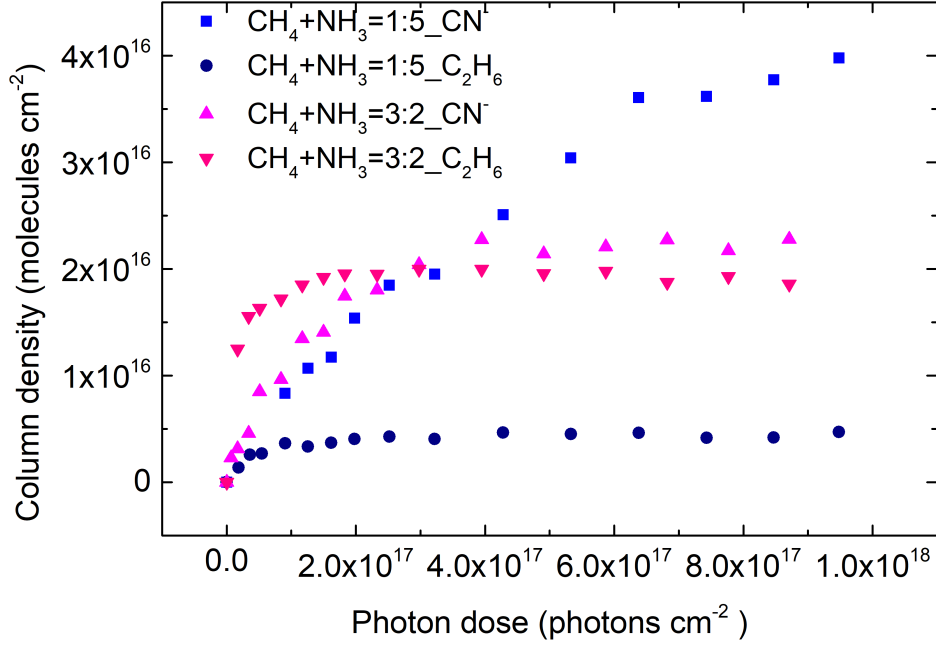
Figure 3.11: The column density of CN^- and C_2H_6 accumulated when different relative proportions of $CH_4 + NH_3$ ice mixtures are irradiated by VUV photons provided by MDHL.

Bossard et al. (2015) [?] is the first to used MDHL to irradiated CH_4 ice at 20 K and a Laser Desorption Post-Ionization Time-Of-Flight mass spectra to find the fragmentation of CH_4. It consist of 95%±5 of CH_3, 4%±1 of CH_2 and 2%±1 of CH. Second, an EUV fragmentation experiment done by Tsai and Eland [?] used 30.4 nm to photo-dissociate CH_4 and tested it by time−of−flight mass spectrometer yields CH_3^+: CH_2^+: CH^+: $C^+ = 1 :0.32: 0.118: 0.0237$ (Tsai 1980). EUV photodissociation experiments of Tsai and Eland (1980)[?] consists of more CH_2 than VUV. Based on these two experimental results, we may conclude that fragment yields of CH_4 dissociation is photon energy dependent and more CH_2 is obtained in EUV range based on gas phase EUV experiment. We aware that the VUV absorption spectra of CH_4 in solid phases is different from gaseous phases [?], and the EUV spectra have not yet measured (without an appropriate window). However, the exact photo dissociation fragmentation ratios by EUV irradiations

in solid state CH$_4$ is still unknown. It is worthwhile for us to perform the experiment by EUV irradiation to see if EUV irradiation can generate any new products on the surface of Charon, or any difference in yield.

Table 3.6 shows the identified peaks of CH$_4$ + NH$_3$ ice mixtures irradiated by VUV and EUV (30.4 nm) irradiated in IR spectra (figure 3.12).

Table 3.6: The peak positions of identified substances after VUV and EUV irradiations in different relative proportions of ice mixtures.

Literture assignments		CH$_4$:NH$_3$ ratio (MDHL)		CH$_4$:NH$_3$ ratio (30.4 nm)		
Wavenumber	Identified IR modes	1:5	3:2	1:5	3:2	Ref.
(cm^{-1})		(cm^{-1})	(cm^{-1})	(cm^{-1})	(cm^{-1})	
3375	ν_3 (NH$_3$)	3366	3367	3368	3368	1
3210	ν_1 (NH$_3$)	3207	3205	3209	3205	1
2972	ν_{10} (C$_2$H$_6$)	2975	2975	2977	2976	3
2960	C$_3$H$_8$	-	2960	-	2960	7
2941	$\nu_8 + \nu_1 1$ (C$_2$H$_6$)	2940	2940	-	2942	3
2904	ν_1 (CH$_4$)	2901	2901	2901	2901	5
2879	ν_5 (C$_2$H$_6$)	2882	2882	-	2884	3
2814	$\nu_2 + \nu_4$ (CH$_4$)	-	2815	-	2813	5
2083	ν (CN$^-$)	2088	2088	2090	2089	2
1625	ν_4 (NH$_3$)	1625	1631	1627	1631	1
1514	δ (NH$_2$)	1509	1511	1509	1511	6
1465-1440	deform CH$_2$ scissor	1461	1463	-	1465	3,4
1390-1370	CH$_3$ sym deform	1394	1372	-	1372	4
1298	ν_4 (CH$_4$)	1301	1299	1303	1301	2
1075	ν_2 (NH$_3$)	1073	1072	1070	1068	1
820	$\nu_1 2$ (C$_2$H$_6$)	-	820	-	-	3

Reference: 1. Bossa et al. (2008) [?] 2. Moore and Hudson (2003) [?] 3. Kim et al. (2010) [?] 4. Socrates et al. (2001) [?] 5. Bennet and Kaiser (2007) [?] 6. Zheng et al. (2008) [?] 7. Hudson and Moore (2004) [?]

From figure 3.13, more C$_3$H$_8$ relative to C$_2$H$_6$ is produced by 30.4nm (40.8 eV) photons than by VUV photons. Considering the formation mechanisms of C$_2$H$_6$ and C$_3$H$_8$, equation (3.2 and 3.4), when MDHL VUV irradiation is replaced by He II 30.4 nm monochromatic light, the ratio of C$_3$H$_8$ to C$_2$H$_6$ in CH$_4$:NH$_3$ = 3:2 ice mixtures irradiated by VUV irradiation is lower than that under EUV provided by NSRRC (figure 3.13).

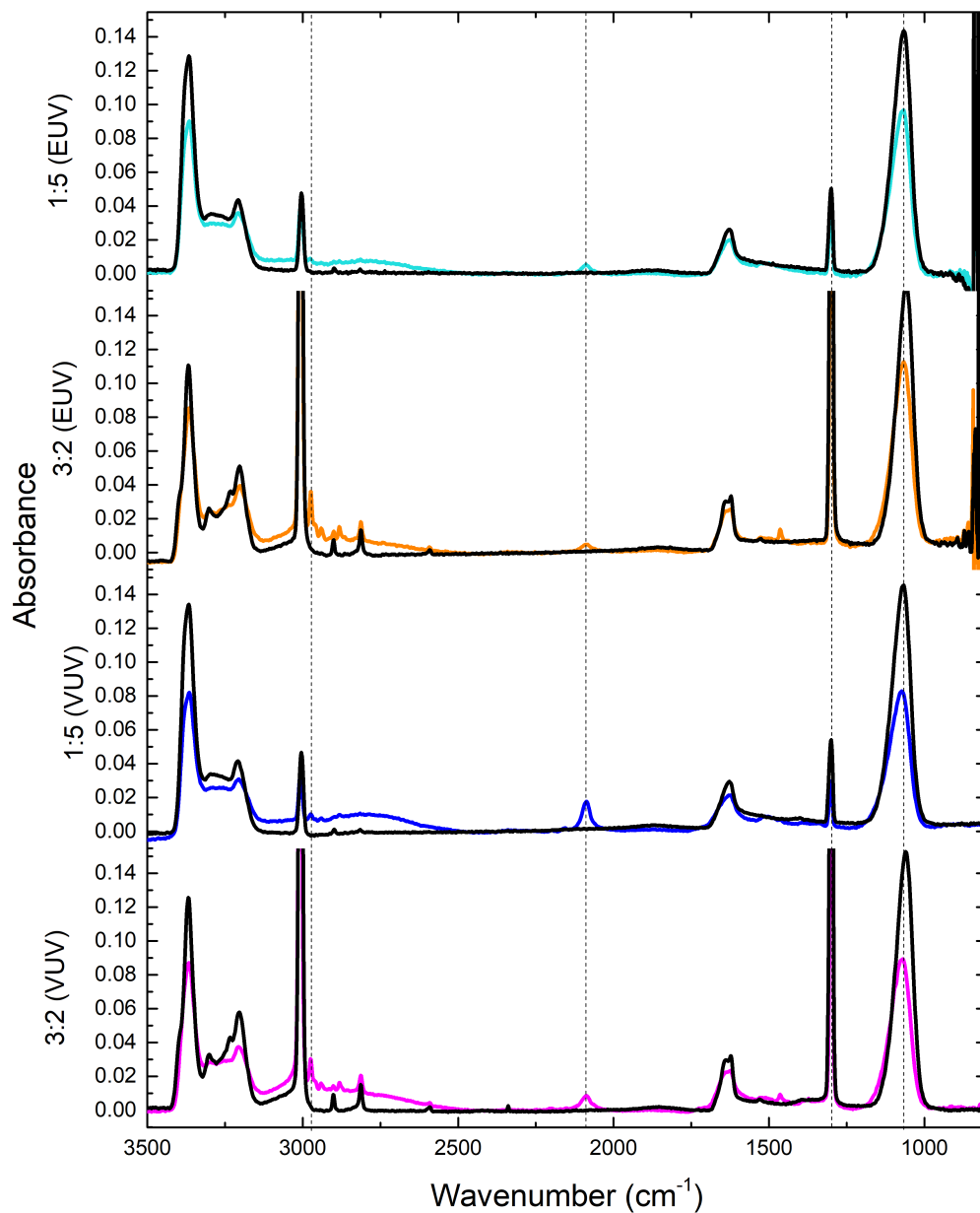**However, our results shows more C$_3$H$_8$ is formed when we use EUV photons as irradiation source. Note that the peak**

Figure 3.12: The infrared spectrum of CH$_4$ + NH$_3$ ice mixtures before irradiation (black),VUV or EUV (coloured) irradiated ice mixtures provided by MDHL and NSRRC. From top to bottom: EUV irradiated CH$_4$:NH$_3$ = 1:5 and 3:2 ice mixtures and VUV irradiated CH$_4$:NH$_3$ = 1:5 and 3:2 ice mixtures.
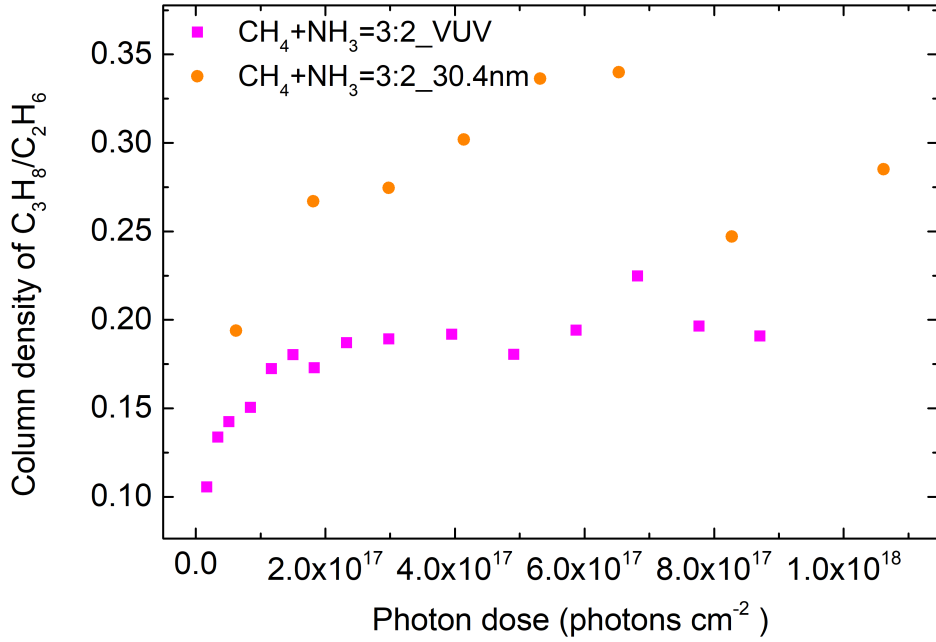
Figure 3.13: The column density of C_3H_8 divided by C_2H_6 accumulated when different relative proportions of $CH_4 + NH_3$ ice mixtures are irradiated by VUV and EUV photons

C_3H_8 is only an tentative assignment which consists of longer carbon chain substances like butane and hexane. The VUV irradiation experiments of CH_4 done by Bossa et al. (2015)[?] at 20 K has shown that the fragments of CH_4 in solid phase consist of 95%±5 of CH_3, 4%±1 of CH_2 while that CH_3 is much more abundant than CH_2 in solid state and agrees well with our experimental results. Hence, methane fragmentation differs in solid state with only 4% of CH_2 and the CH_2 to CH_3 ratio should increase when EUV photons are adopted.

W

Table 3.7: The fitting results of reactants by equation $[R] = [R]e^{-kx} + C$

Constituent	VUV (photon^{-1}cm^2)	EUV (photon^{-1}cm^2)	ratio of k in VUV/EUV
CH_4	3.70 ± 0.18	0.61 ± 0.03	6.06 ± 0.07
NH_3	2.89 ± 0.10	0.91 ± 0.11	3.18 ± 0.12

Apart from C_2H_6 and C_3H_8, CN^- production may differ. Figure 3.15 shows the accumulated column densities of CN^- generated by ir-
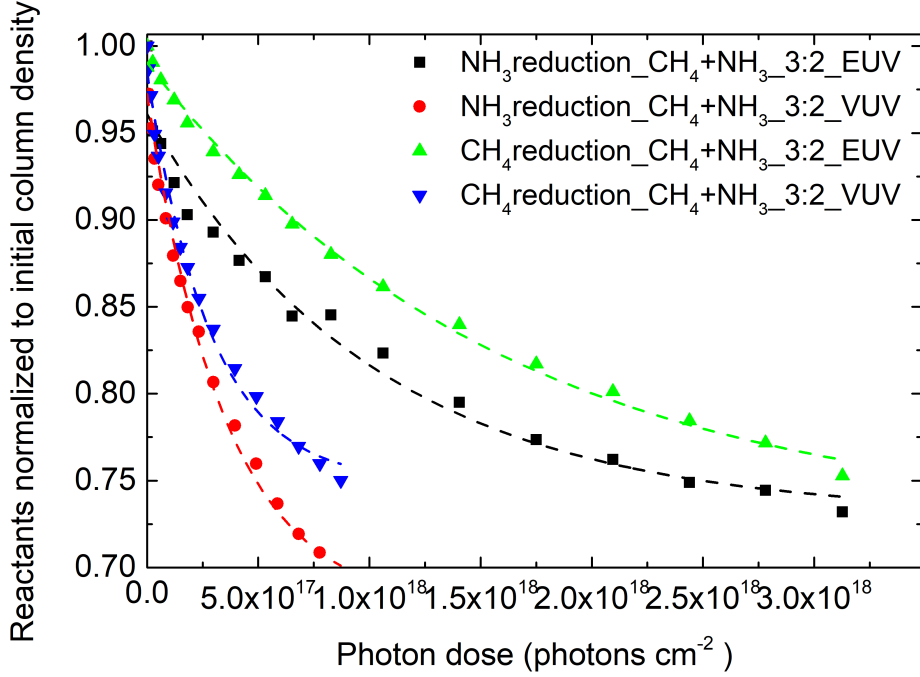
34

Figure 3.14: The normalized destruction of CH_4 and NH_3 in $CH_4 + NH_3$ ice mixtures irradiated by VUV and EUV photons

radiation of CH_4+NH_3 ice mixtures by MDHL and 30.4 nm monochromatic light. The fitting results are shown in Table 3.6. The rate constants forming CN^- is 3.06 to 4.13 times larger in CH_4:NH_3 = 1:5 and 3:2 irradiated by MDHL than irradiated by 30.4 nm monochromatic light respectively. We fit the column densities of CH_4 and NH_3 ice mixtures which are normalized by the deposited column densities (figure 3.14) with pseudo first order decay equation, the destruction cross-section of CH_4 and NH_3 are reduced by 6.06±0.07 and 3.19±0.12 times respectively (table 3.7). The formation rate constant of CN^- is 3.06 to 4.13 times smaller than VUV irradiations (table 3.8. Therefore, we may conclude that the decrease in CN^- formation rate by 30.4nm (40.8 eV) EUV irradiation is mainly due to the decreased NH_3 destruction cross-sections. In general, the energy of MDHL has already exceeded the energy required to form the CH_3 and NH_2 radicals, further increasing photon energy would not pose dramatical change to CH_4 and NH_3 ice mixtures.
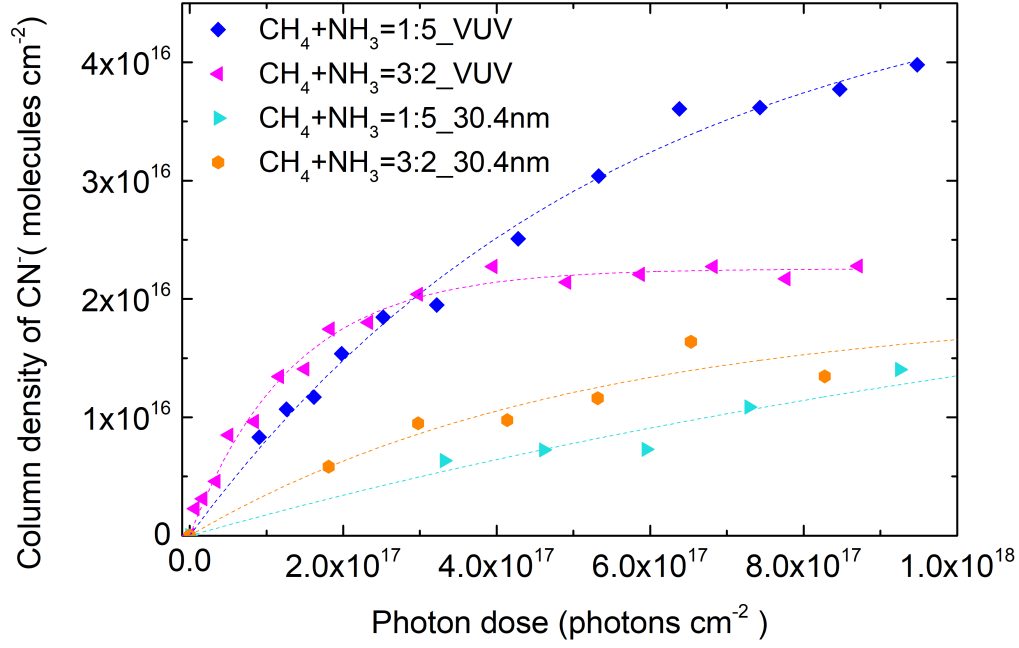
Figure 3.15: The column densities of CN^- generated by irradiation of CH_4+NH_3 ice mixtures by MDHL and 30.4 nm monochromatic light.

Table 3.8: The fitting results of CN^- by equation 2.10

Light source	Ratio of CH_4:NH_3	A (x10^{16} molecules cm^{-2})	k_1 (x10^{-18} photon^{-1})	k_2 (photon^{-1})
VUV	1:5	4.61 ± 0.18	1.93 ± 0.19	>1
MDHL	3:2	2.24 ± 0.03	8.21 ± 0.70	>1
EUV	1:5	2.89 ± 1.29	0.63 ± 0.37	>1
30.4nm	3:2	2.24 ± 0.03	1.92 ± 1.99	>1

Fitting result of figure 3.15 with pseudo first order equation $[CN^-]=A(1-e^{-kx})$. These fitting results of MDHL experiments are an average of at least 2 experiments with the same circumstances. In the expression, A represents the column density when x, the photon dose, becomes infinitely large and k is the rate constant.

3.5 Residues

The residues we studied are the accumulated substances remained on the substrate after warmed up. Figure 3.16 is a comparison of CH_4:NH_3 = 3:2 after VUV experiments, residues accumulate after EUV exposure of CH_4:NH_3 = 3:2 ice mixtures and the plasma experiment done by Imanaka et al. (2004)[?]. The peak positions and assignments are listed at table 3.9. The residues formed in irradiated ammonia dominating CH_4+NH_3 ice mixtures are not observed after accumulation of consecutive experiments. There are no differences between EUV accumulated residues and VUV accumulated residues in CH_4:NH_3 = 3:2 ice mixtues. The main functional groups (nitrogen position) of the residues are conjugated nitriles. Based on experiments of N_2+CH_4 (9:1) done at 2300 Pa. by Imanaka et al. (2004)[?], the tholins formed at high pressure (2300 Pa) should be a polymer-like branched chain structure terminated with -CH_3 -NH_2 and -C$\equiv$N with few aromatic compounds.

Table 3.9: The peak positions of residues and their assignments

Imanaka et al. (2004) ν (cm^{-1})	implied functional group	VUV (MDHL) ν (cm^{-1})	EUV (30.4 nm) ν (cm^{-1})
2954 - 2972	-CH_3- asymmetric stretching	2955	2962
2929 - 2932	-CH_2- assymmetric stretching	2923	2929
2869 - 2874	-CH_3- symmetric stretching	2871	2871
2173 - 2189	conjugated nitriles, such as with -C=C(-NH_2) C-N$\equiv$C stretching	2173	2174
1460	C-CH_3 asymmetric bending	1451	1451
1375-1379	C-CH_3 unbrella symmetric bending	1372	1378

Similar residues is obtained by using different initial reactants (replacing N_2 by NH_3). The similarities during formation of atomic nitrogens when breaking N$\equiv$N bonds in nitrogen molecules (N_2) and N-H bonds in ammonia give rise to this result. When photon energy is enough to break both NH bond and N$\equiv$N bond, similar experimental residues forms. Our results implies that the residues formed on Charon is similar to what they found on Titan, although their formation environments differs from gaseous phase with N_2 dominating to solid phase with NH_3.
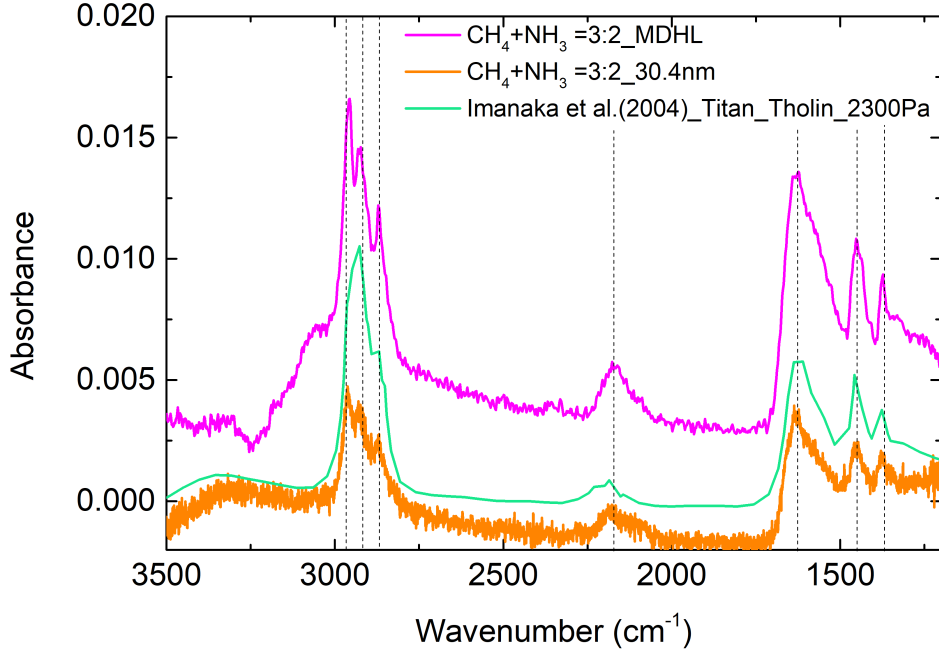
Figure 3.16: **IR spectra of accumulated residues of CH$_4$:NH$_3$=3:2 ice mixtures irradiated with VUV photons which provided by MDHL(pink solid line) and monochromatic EUV photons which provided by NSRRC (orange solid line).**

3.6   Summary

The main product of VUV and EUV irradiated CH$_4$+NH$_3$ ice mixtures were C$_2$H$_6$ and CN$^-$. C$_3$H$_8$ was also produced by C$_2$H$_6$ or C$_2$H$_2$. We did several investigations towards CH$_4$+NH$_3$ ice mixtures. First, by changing ratio of CH$_4$ to NH$_3$ ice mixtures, CN$^-$ production was more effective in NH$_3$ dominated ice mixtures. While in contrast, C$_2$H$_6$ wss the main product when CH$_4$ dominates. Second, by changing the photon source to EUV irradiation, the difference in photo-production yield was mainly caused by the decrease in photo-destruction cross-section in the reactants. Finally, we compared our residues obtained with laboratory produced Titan tholins, the similar infrared spectrum showed a similar functional groups in residues. Our result implied that the tholin on Charon should be similar to that of Titan.

4. Astrophysical Implications